PHYSICAL REVIEW B **70**, 045316 (2004)

Near-band-gap dielectric function of $Zn_{1-x}Mn_xSe$ thin films determined by spectroscopic ellipsometry

J. Kvietkova,* B. Daniel, and M. Hetterich
Institut für Angewandte Physik and Center for Functional Nanostructures (CFN), Universität Karlsruhe, Wolfgang-Gaede-Str. 1, D-76131 Karlsruhe, Germany

M. Schubert and D. Spemann
Intitut für Experimentelle Physik II, Fakultät Für Physik und Geourssenschaften, Universität Leipzig, Linnéstr. 5, D-04103 Leipzig, Germany

D. Litvinov and D. Gerthsen
Laboratorium für Elektronenmikroskopie and CFN, Universität Karlsruhe, D-76128 Karlsruhe, Germany

(Received 16 February 2004; revised manuscript received 20 April 2004; published 26 July 2004)

We present a study of the optical properties of cubic $Zn_{1-x}Mn_xSe$ thin films with $x=0, 0.136$ and 0.21, grown on GaAs(001) substrates by molecular beam epitaxy. We determine the complex dielectric function using variable-angle spectroscopic ellipsometry in the photon energy range from 0.75 to 4.5 eV. A critical-point parametric model including the two lowest critical points E_0 and $E_0+\Delta_0$ is employed for the dielectric function. An excellent match of the experimental data is obtained in the below and near-band-gap photon energy range. For increasing Mn content we observe a large negative bowing of the band gap and an increase in the spin-orbit splitting (by 80% for 21% Mn). From the fit, an exciton binding energy of 17 meV is obtained for ZnSe. This value changes only slightly with the addition of Mn, namely to 17 and 20 meV for 13.6% and 21% Mn, respectively. The below-band-gap index of refraction is well represented by a simple Cauchy dispersion formula, which is provided here as well.

DOI: 10.1103/PhysRevB.70.045316 PACS number(s): 78.20.Ci, 78.66.Hf

I. INTRODUCTION

ZnSe related semiconductor materials have already been successfully applied in a variety of optoelectronic devices, e.g., in photodetectors and light sources for the UV, blue and green spectral region,[1] or in electro-optic waveguide modulators.[2] Recently, $Zn_{1-x}Mn_xSe$ attracted large attention as a suitable spin aligner for future spin-based electronic device structures.[3] The addition of the 3*d*-transition element manganese to ZnSe leads to expected changes of the electronic and optical properties. A nonlinear dependence of the band gap energy on the Mn concentration has been reported and was studied in detail by several authors.[4–8] This phenomenon, observed also in other diluted magnetic semiconductors (e.g. in $Cd_{1-x}Mn_xS^9$),[9] has been attributed to the large electronic *sp-d* exchange interaction between the magnetic-element-induced states and the host conduction and valence band states.[10]

Electronic properties, such as the band-to-band transition energies, strength, and broadening parameters, are strongly related to the dielectric function ϵ. Hence, knowledge of ϵ provides access to fundamental physical material parameters. The index of refraction (n) and the absorption coefficient (k) follow directly from $\epsilon=(n+ik)^2$, $i=\sqrt{(-1)}$. The knowledge of the material parameters n and k is crucial for the design of the optoelectronic devices. However, investigations of the dielectric function of $Zn_{1-x}Mn_xSe$ at optical wavelengths, specifically in the near-band-gap spectral region have not been exhaustive so far. Adachi and Taguchi[11] reported on spectroscopic ellipsometry (SE) studies of ZnSe. A simplified model for the electronic band-to-band transition contributions was employed, which led to fair agreement with the experimental data. Dahmani *et al.*[12] used a set of harmonic oscillators to fit the SE measurement. In both reports, the effects of the native surface overlayer, which forms naturally on the ZnSe surface under normal ambient, were ignored in the data analysis. The latter was taken into account in Ref. 13 where a much better agreement between experiment and theory is obtained. This, however, was achieved using a rather complicated model with a large number of fit parameters. This model was based on the analytical construction of the joint density of states and the use of both Lorentzian and Gaussian line broadening.

Several authors presented the dielectric function of ZnMnSe with different Mn content, but only for photon energies $E=\hbar\omega$ from 3.5 to 5.5 eV,[14,15] i.e., above the fundamental band-to-band transition energy. Within the band gap, to our knowledge, the refractive index for $Zn_{1-x}Mn_xSe$ with Mn contents up to 46% was determined for a single wavelength only ($\lambda=632.8$ nm).[16]

In this paper we report on the dielectric function of $Zn_{1-x}Mn_xSe$ obtained by spectroscopic ellipsometry (SE) in the energy range 0.75–4.5 eV. We provide a model dielectric function parameter set for a calculation of the dielectric function, including an approximate parameter representation of the below-band-gap index of refraction dispersion. We discuss the dependence of the two lowest critical-point energies E_0 and $E_0+\Delta_0$ on the Mn content. Special attention is given to an unexpectedly large increase in the spin-orbit splitting with growing Mn concentration.

II. EXPERIMENTAL DETAILS

$Zn_{1-x}Mn_xSe$ films in the cubic zinc blende modification were grown by molecular-beam epitaxy on GaAs(001) substrates using Zn, Mn and Se as source materials. In order to control the composition, only the Mn flux was varied while the fluxes of the other two elements were held constant. Slightly Se-rich growth conditions were used in all cases to ensure a good crystal quality. Depending on composition, the growth rate ranged from 255 to 380 nm/h. For each composition one pair of samples with thicknesses of about 700 and 1400 nm was prepared. On top of the Mn-containing samples a thin (5 nm) ZnSe cap layer was added. In order to determine the manganese content in each sample as accurately as possible, we used Rutherford backscattering (RBS), particle-induced x-ray emission (PIXE), and energy-dispersive x-ray analysis (EDX). The results from all these methods were in good agreement. For the three pairs of samples used in the optical experiment the Mn concentrations were 0%, 13.6%, and 21%, respectively. All samples were found to be stoichiometric within the experimental resolution.

The structural properties of the samples were studied by transmission electron microscopy (TEM). Figure 1 shows [110] cross-section bright-field TEM images of the ZnSe (a) and $Zn_{0.864}Mn_{0.136}Se$ (b) sample, respectively, taken under two-beam conditions with imaging vector $\mathbf{g}=(002)$. In the Mn-containing layer stacking faults with a density of $\sim 100\ \text{cm}^{-2}$ are found, which is a well known problem of this material system. However, as proven by TEM diffraction patterns (see, e.g., insets in Fig. 1) all samples investigated have the zinc blende crystal structure.

A spectroscopic rotating-analyzer ellipsometer with automated compensator function (J.A. Woollam Co.) was used for ellipsometry measurements in the photon energy range from 0.75 to 4.5 eV. The spectral resolution was 10 meV, and data were acquired at angles of incidence $\Phi_a=76°$ and 78°.

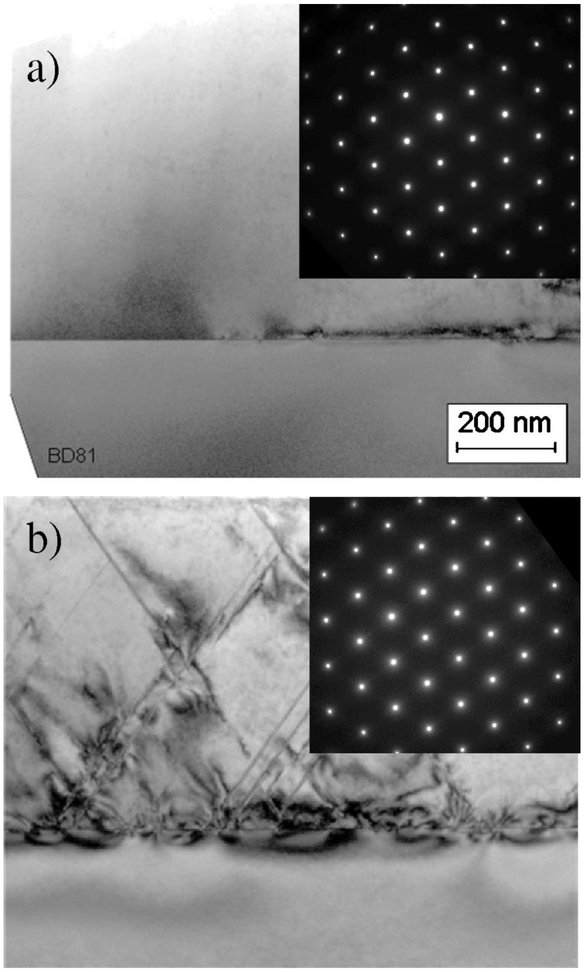

FIG. 1. [110] cross-section bright-field TEM images of the ZnSe (a) and $Zn_{0.864}Mn_{0.136}Se$ (b) samples with corresponding diffraction patterns in the insets.

III. ELLIPSOMETRY DATA ANALYSIS

A. Ellipsometry

Ellipsometry can determine the complex dielectric function ϵ and thickness d of a thin-film sample by comparing the measured data with best-fit model calculations. The standard ellipsometric parameters are defined through Ψ and Δ. They are related to the complex reflectance ratio ρ,[17]

$$\rho \equiv \frac{r_p}{r_s} = \tan \Psi \exp(i\Delta), \tag{1}$$

where r_p and r_s are the reflection coefficients for light polarized parallel (p) and perpendicular (s) to the plane of incidence, respectively. The ellipsometric parameters depend on the photon energy E, the sample layer structure (layer sequence and thickness d), the dielectric function ϵ of all materials involved, and the angle of incidence Φ_a. The pseudodielectric function $\langle\epsilon\rangle$ is a common representation of the ellipsometric data Ψ and Δ assuming the two-phase (ambient-substrate) model,[18]

$$\langle\epsilon\rangle = \epsilon_a([(1-\rho)/(1+\rho)]^2\sin^2\Phi_a + \cos^2\Phi_a)\tan^2\Phi_a, \tag{2}$$

where the ambient dielectric function $\epsilon_a=1$.

B. Data analysis

Ellipsometry is a model-based technique and experimental data must be compared with model calculations. One way to obtain the optical constants of the layer of interest is the wavelength-by-wavelength ("point-by-point") numerical inversion of the experimental data.[19] The point-by-point fit is normally inapplicable to single sample data analysis, because of the correlation problem between ϵ and d within the spectral region where the thin film is transparent. If, however, (i) all other material constituents optical constants are known, and (ii) samples with thin films of sufficiently different thickness but equal material properties are available, the point-by-point fit is fully applicable (multiple sample analysis). In addition to the thickness and the real and imaginary values of ϵ for each photon energy, we included the thickness and the Lorentz function parameters of the oxide overlayer, as discussed in Sec. III D. Alternatively, the number of unknown parameters for data analysis can be reduced if appropriate parametric line shape functions for the materials of interest are available. Such model dielectric function approaches were also applied, as discussed below.

A regression analysis is commonly used to vary the model parameters until the calculated $(\Psi^c_{ij},\Delta^c_{ij})$, and measured (Ψ_{ij},Δ_{ij}) data match as closely as possible. This is done by minimizing the mean-square error (MSE) function, which is appropriately weighted to the estimated experimental errors $\sigma_{ij}{}^{\Psi}$ and $\sigma_{ij}{}^{\Delta}$ (Ref. 20),

$$\mathrm{MSE}=\frac{1}{2MN}\sum_{i,j}^{N,M}\left[\left(\frac{\Psi_{ij}-\Psi^c_{ij}}{\sigma_{ij}{}^{\Psi}}\right)^2+\left(\frac{\Delta_{ij}-\Delta^c_{ij}}{\sigma_{ij}{}^{\Delta}}\right)^2\right]. \qquad (3)$$

The indices i and j indicate (Ψ,Δ) data sets at photon energy E_i and angle of incidence Φ_{aj}.

C. Model dielectric function

For SE data analysis simple parametric optical functions such as the Cauchy model for dielectrics, or the Zollner model for semiconductor native-oxides[21] are often utilized.[20] General parametric models, i.e., model dielectric functions (MDF), that completely describe critical point (CP) structures and the line shape of the dielectric function of semiconductors are highly complex, and have been developed, e.g., by Kim *et al.*.[22] and Kim, Garland, and Raccah.[23] Such models reveal information about CP energy, broadening, and the joint density of states. Accurate CP energies and linewidths are then obtained from analysis of SE data and its derivatives.[23,24] Based on the one-electron parabolic-band approximation and augmented by discrete and continuum excitonic contributions, Adachi's composite MDF has often been applied with success to numerous semiconductor compound materials.[25] In this model the dielectric function is given as a sum of contributions of individual CP structures,

$$\epsilon=\epsilon_{E_0}+\epsilon_{E_0+\Delta_0}+\epsilon^{d.e.}_{E_0}+\epsilon^{d.e.}_{E_0+\Delta_0}+\epsilon^{c.e.}_{E_0}+\epsilon_C. \qquad (4)$$

The expressions for all parts of Eq. (4) are given in the following.

The E_0 and $E_0+\Delta_0$ transitions are of the three-dimensional (3D) M_0 type. Assuming parabolic bands they are described by

$$\epsilon_j(E)=e^{i\phi_j}A_jE_j^{-1.5}\chi_j^{-2}[2-\sqrt{1+\chi_j}-\sqrt{1-\chi_j}], \qquad (5)$$

with $\chi_j=(E+i\Gamma_j)/E_j$ ("j" = "E_o", "$E_o+\Delta_0$"). A_j, E_j, and Γ_j denote, respectively, amplitude, transition energy, and broadening (lifetime) parameter of the CP transition. The constant-complex-phase parameter ϕ accounts for coupling between spectrally adjacent resonance transitions, rendering the effects of Lorentzian-broadened anharmonic line shape functions. The excitonic transitions in the vicinity of the lowest direct band gap have a strong influence on the optical properties. The contributions due to discrete excitons (d.e.) are given by a Lorentzian line,

$$\epsilon^{d.e.}_j(E)=e^{i\phi^{d.e.}_j}A^{d.e.}_j/(E_j-E_{eb}-E-i\Gamma^{d.e.}_j), \qquad (6)$$

with E_{eb} being the exciton binding energy ("j" = "E_o", "$E_o+\Delta_0$," respectively). The continuum-exciton (c.e.) transitions are modeled with a Lorentz oscillator,

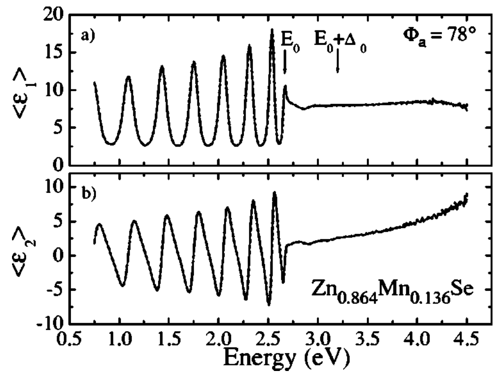

FIG. 2. Real (a) and imaginary (b) parts of the pseudodielectric function $\langle\epsilon\rangle$ of the sample with 700 nm of $Zn_{0.864}Mn_{0.136}Se$. Dashed lines denote the experimental data and solid lines show the best-fit calculated data obtained by the point-by-point fit approach.

$$\epsilon^{c.e.}(E)=A^{c.e.}E^{c.e.}\Gamma^{c.e.}/((E^{c.e.})^2-E^2-i\Gamma^{c.e.}E). \qquad (7)$$

Contributions from higher-energy CP transitions outside the spectral range of our experiment are modeled by

$$\epsilon_C(E)=\epsilon_s+A_p/(E_p^2-E^2), \qquad (8)$$

where ϵ_s is a constant offset and A_p and E_p are amplitude and position of a loss-less dispersion pole, respectively.

D. Layer model

A four-layer model (three-layer for the ZnSe samples) was used here for the analysis. This model consists of the GaAs substrate, the $Zn_{1-x}Mn_xSe$ layer, the ZnSe cap layer (except for the ZnSe samples), and the native ZnSe oxide overlayer. The optical properties of the ZnSe native oxide are not known. Koo *et al.*[26] modeled this overlayer by the use of the Bruggeman effective-medium approach averaging the optical constants of amorphous Se, $(Ga,As)_2O_3$, and the ambient. In our model we applied a simpler approach, which is based on the semiconductor oxide optical constants model introduced by Zollner.[21] Accordingly, the dielectric function of the ZnSe native oxide is described here by a Lorentz oscillator function, and its parameter values together with the oxide thickness d_{ox} were varied during the best-fit data analysis. We obtained $d_{ox}\sim 3$ nm for all samples, similar to the results reported in Ref. 26.

IV. RESULTS AND DISCUSSION

Figure 2 depicts, as an example, the real (a) and imaginary (b) part of the pseudodielectric function for the sample with 13.6% manganese and a thickness of 700 nm. The experimental data (dashed line) are shown along with the best-fit results obtained by the point-by-point multiple sample analysis approach (solid line). The two spectra are in excellent agreement.

Note that in the fit procedure a small thickness inhomogeneity of about 2% for all layers has been taken into ac-

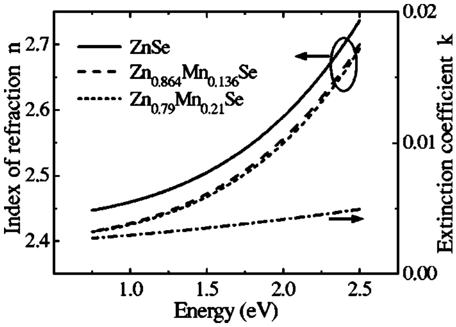

FIG. 3. The index of refraction for $Zn_{1-x}Mn_xSe$ obtained from the best-fit analysis of the below-band-gap experimental data by use of the Cauchy dispersion model.

count as well as a nonzero (<2 nm) spectral bandwidth of the detection system.

A. Below-band-gap index of refraction

To begin with, the ellipsometry data in the below-band-gap spectral region (0.75–2.5 eV) were analyzed by using the Cauchy model function for parametrization of the $Zn_{1-x}Mn_xSe$ index of refraction. Thereby, the following formula was used:

$$n(\lambda) = A + \frac{B}{\lambda^2} + \frac{C}{\lambda^4}, \tag{9}$$

where $\lambda = 2\pi c/\omega$ denotes the wavelength, c is the speed of light, and A, B, and C are the Cauchy model parameters. For the sample with 21% manganese considerable absorption was present, and the extinction coefficient k needed to be included. This was done by the following approximation (exponential absorption tail):

$$k(\lambda) = \alpha \exp\left[\beta\left(\frac{hc}{\lambda} - \gamma\right)\right], \tag{10}$$

where α is the amplitude, β the exponent factor, γ the band edge in eV, and h Planck's constant. Note, that Eqs. (9) and (10) are not Kramers-Kronig consistent.

Figure 3 shows the resulting index of refraction and extinction coefficient spectra. The best-fit calculation parameters are listed in Table I. We observe a considerably smaller refractive index change upon the incorporation of manganese in ZnSe than that reported previously upon the incorporation of Cd or Mg.[16] The index of refraction decreases with increasing Mn composition. The same trend is reported in Ref. 16, where the index of refraction was measured for a single wavelength using the prism coupling technique. However, our values are somewhat lower (by 1%). This might be due to the assumption of slightly incorrect thickness values, which are potential error sources for the prism method.

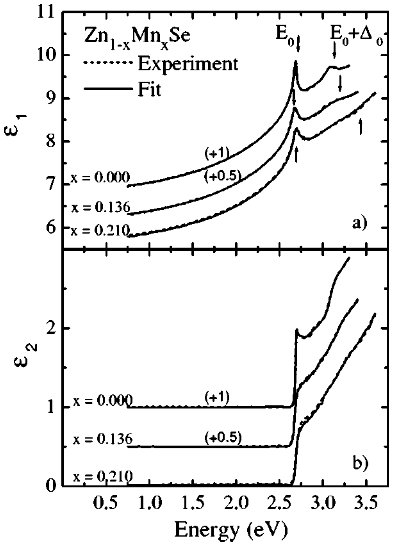

FIG. 4. The real (a) and imaginary (b) part of the dielectric function of $Zn_{1-x}Mn_xSe$. The dotted lines correspond to the wavelength-by-wavelength inverted ellipsometry data and the solid lines to the modeled spectra. For clarity, the spectra are shifted by 0.5 for $Zn_{0.864}Mn_{0.136}Se$ and by 1 for ZnSe.

B. $Zn_{1-x}Mn_xSe$ dielectric function (0.75–4.5 eV)

The dielectric function of the $Zn_{1-x}Mn_xSe$ thin films was determined over the spectral range from 0.75 to 4.5 eV by the multiple sample point-by-point inversion approach. In this procedure the thickness values of the individual $Zn_{1-x}Mn_xSe$ layers were taken from the below-band-gap data analysis and held constant. As described above, the thicknesses and parameters of the oxide overlayer as well as the thickness of the ZnSe cap layer were varied. The resulting ϵ spectra for ZnSe, $Zn_{0.864}Mn_{0.136}Se$, and $Zn_{0.79}Mn_{0.21}Se$ are shown in Fig. 4. Our spectra for ZnSe are in very good agreement with data published previously.[11,13] For the other two compositions data are only available in the spectral region from 3.5 to 5.5 eV so far.[14,15] Our ϵ_1 values are slightly higher, whereas the ϵ_2 values are lower than those reported by Hung *et al.*, respectively.[15] This can be attributed to the better description of the oxide overlayer effect in our analysis. Improper numerical reduction by use of inadequate oxide optical constants affects the resulting thin film dielectric function. The effect is a reduction (increase) of the real

TABLE I. Cauchy model parameters [Eqs. (9) and (10)] for the index of refraction of $Zn_{1-x}Mn_xSe$

	A	B(μm^2)	C(μm^4)	α	β	γ(eV)
ZnSe	2.43331	0.03448	0.00991			
$Zn_{0.864}Mn_{0.136}Se$	2.40064	0.03472	0.00961			
$Zn_{0.79}Mn_{0.21}Se$	2.4018	0.02997	0.01029	0.00529	0.34072	2.7

TABLE II. Best-fit MDF parameters for $Zn_{1-x}Mn_xSe$ in the given photon energy range. The values in parentheses refer to the error bar of the last digit and a 90% confidence interval.

x_{Mn}	0	0.136	0.21
E_0(eV)	2.711(1)	2.664(1)	2.671(2)
$A_{E_0}(eV)^{3/2}$	16.5(8)	15.1(9)	16.2(9)
Γ_{E_0}(meV)	3(5)	6(2)	3(2)
ϕ_{E_0}	0.16(3)	−0.11(9)	−0.40(8)
Δ_0(meV)	424(20)	530(60)	760(50)
$A_{E_0+\Delta_0}(eV)^{3/2}$	21(3)	19(3)	35(4)
$\Gamma_{E_0+\Delta_0}$(meV)	11(20)	47(80)	92(88)
$\phi_{E_0+\Delta_0}$	−0.15(4)	0.11(9)	0.25(5)
E_{eb}(meV)	17(2)	17(10)	20(15)
$A_{E_0}^{d.e.}(eV)^{-1}$	0.016(1)	0.02(2)	0.034(30)
$\Gamma_{E_0}^{d.e.}$(meV)	18(1)	81(11)	103(9)
$\phi_{E_0}^{d.e.}$	−0.63(12)	3.1(2)	3.0(3)
$A_{E_0+\Delta_0}^{d.e.}(eV)^{-1}$	0.024(9)	0.023(20)	0.078(60)
$\Gamma_{E_0+\Delta_0}^{d.e.}$(meV)	56(18)	116(84)	183(46)
$\phi_{E_0+\Delta_0}^{d.e.}$	−0.28(36)	0.28(85)	1.28(28)
$E_0^{c.e.}$(eV)	2.73(2)	2.70(1)	2.71(2)
$A_{E_0}^{c.e.}$	0.13(5)	0.48(22)	0.68(30)
$\Gamma_{E_0}^{c.e.}$(meV)	85(40)	163(34)	225(27)
E_p(eV)	4.67(2)	4.69(3)	4.76(7)
$A_p(eV)^2$	39(1)	42(1)	38(2)
ϵ_s	2.21(6)	2.12(7)	1.8(1)
Photon energy range (eV)	0.75−3.3	0.75−3.4	0.75−3.6

(imaginary) part, specifically near band-to-band transition energies, as demonstrated by Aspnes *et al.*[18]

C. Critical-point analysis

The above described critical-point model with 21 parameters has been used for the fit of the measured data. The model comprises only the two critical points with energies within the range of our measurement and the corresponding discrete and continuum exciton contributions. All higher-energy CP are modeled by a single pole function and a constant offset. In order to allow this simplification the photon energy range of the fit was limited to the region from 0.75 eV to just above the $E_0+\Delta_0$ CP, i.e. to 3.3 eV for ZnSe, 3.4 eV for $Zn_{0.864}Mn_{0.136}Se$ and 3.6 eV for $Zn_{0.79}Mn_{0.21}Se$. In this range an excellent agreement was achieved for all three samples as shown in Fig. 4. The experimental dielectric function is given by dotted and the model by solid lines for the three manganese compositions under study (x=0, 0.136 and 0.21). For clarity the spectra are shifted along the y-axis by 0.5 for $Zn_{0.864}Mn_{0.136}Se$ and by 1 for ZnSe. The best-fit values of all parameters are listed in Table II. It should be noted here that the critical-point parameters obtained from the model used in this work will be different from the critical-point parameters determined using different model dielectric function approaches, and different analysis techniques will potentially yield different critical-point parameters.

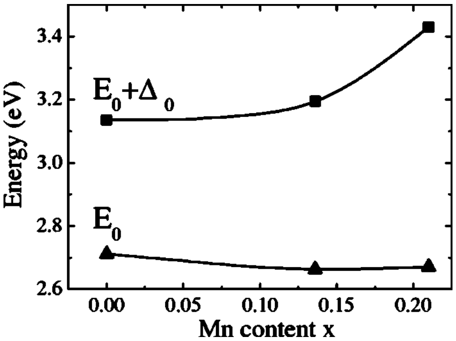

FIG. 5. The position of E_0 and $E_0+\Delta_0$ CP as a function of the Mn content in $Zn_{1-x}Mn_xSe$ as obtained from the MDF fit. (The lines are just a guide for the eye.)

The energy positions of the E_0 (2.71 eV) and $E_0+\Delta_0$ (3.14 eV) CP of ZnSe obtained from the fit are almost identical with those presented in Refs. 13 and 27. The values from other authors (e.g., Refs. 11, 12, and 14) are slightly lower.

The dependence of these two energies on the Mn content in our $Zn_{1-x}Mn_xSe$ samples is shown in Fig. 5. (The connecting lines are just a guide for the eye.) The lowest E_0 CP exhibits at first a redshift and then a blueshift with increasing Mn concentration, which is in agreement with the band gap anomaly caused by the *sp-d* exchange interaction observed already in photoreflectance, absorption, and photoluminescence measurements.[8–10] The $E_0+\Delta_0$ CP, on the other hand, does not seem to follow this behavior. With increasing Mn concentration the spin-orbit splitting is increasing quite significantly, from 424 meV in ZnSe to 760 meV for 21% manganese. One possible cause we considered to be responsible for this increase is the effect of the strain in the Mn-containing samples on the band structure. However, using the formulas in Ref. 28, the ZnSe deformation potential values from Ref. 29 and the elastic constants for ZnMnSe from Ref. 30, it can be estimated that strain has only a small influence on the spin-orbit splitting. In an extreme case of fully strained epilayers, the in-plane and vertical strains for the sample with 21% Mn would be −0.0085 and 0.0107, respectively, and the resulting change in the spin-orbit splitting would be only 25 meV. At the same time the change in the band gap due to strain would be only 12 meV, which is four times smaller and of an opposite sign than the change obtained from the fit. Therefore, we conclude that strain cannot be responsible for the observed band gap anomaly. Moreover, x-ray diffraction measurements showed that the residual strain in our samples is actually much smaller (see Ref. 30 for details). For the sample with 43% Mn investigated in Ref. 30 the strain would lead to a shift of the spin-orbit split-off band by less than 20 meV. Therefore, the small residual strain present in the samples accounts only for a minor increase in the spin-orbit splitting. We suggest that a possible reason for the observed strong increase is—apart from the anomalous composition dependence of E_0—the influence of the high angular momentum 3*d* Mn states on the ZnSe valence band wavefunction.

It is also interesting to note that while the broadening of the E_0 transition stays almost the same (below 10 meV) for all three samples, the transition at the $E_0+\Delta_0$ CP is considerably broadened with increasing Mn concentration. The broadening of the continuum exciton transition is also enlarged; for 21% Mn it is about three times larger than in ZnSe. This contribution lies approximately 20 meV above the band gap in ZnSe and follows the shift of the E_0 CP with an increasing Mn concentration.

The exciton binding energy E_{eb} of ZnSe has been studied by several authors. A value of 19 meV derived from low temperature magnetoreflectance measurements was reported in Ref. 31. In this publication similar results of other authors are cited. In the more recent paper of Lee *et al.*[32] a larger value of 22 meV has been determined from magnetoabsorption measured at the liquid helium temperature. Kim *et al.*,[13] on the other hand, found an exciton binding energy of 13 meV. This was obtained from the fit of the room temperature ellipsometry data. The authors explained their lower value to be due to the temperature dependence of the dielectric function and of the effective mass. Our fit yields E_{eb} of $\sim$17 meV for ZnSe. Taking into account the experimental error bar, this value is in a fairly good agreement with the previous low temperature results. Slight deviations might be due to the temperature-dependence of the combined exciton effective mass. With the addition of Mn, E_{eb} stays almost unchanged, i.e., 17 meV for $\mathrm{Zn}_{0.864}\mathrm{Mn}_{0.136}$Se and $\sim$20 meV for $\mathrm{Zn}_{0.79}\mathrm{Mn0}_{0.21}$Se..

V. CONCLUSIONS

We presented the complex dielectric function of $\mathrm{Zn}_{1-x}\mathrm{Mn}_x$Se ($x=0$, 0.136, and 0.21) for photon energies from 0.75 to 4.5 eV extracted from the point-by-point fit of the ellipsometric measurements. For the case of ZnSe very good agreement with other published experimental curves[11,13] was found. In the transparent region the Cauchy model parameters for the refractive index of $\mathrm{Zn}_{1-x}\mathrm{Mn}_x$Se were given. The refractive index decreases with growing Mn content, consistently with the results in Ref. 16.

The experimental dielectric function of $\mathrm{Zn}_{1-x}\mathrm{Mn}_x$Se was fitted with high accuracy in the photon energy range from 0.75 to 3.3 eV using a critical-point parametric model. Especially in the vicinity and below the band gap an improved agreement was achieved with our MDF compared to previously published models.

The fit yields the positions of the two lowest CP E_0 and $E_0+\Delta_0$. These energies show a different dependence on the Mn content. With increasing Mn concentration we found a large negative bowing of the band gap observed already in photoluminescence and photoreflectance measurements.[8–10] The $E_0+\Delta_0$ CP, on the other hand, shifts to higher energies. The unexpectedly strong increase in the spin-orbit splitting Δ_0 may be related to the anomalous composition dependence of E_0 and the admixture of 3*d* Mn states with high angular momentum to the valence band wavefunction.

ACKNOWLEDGMENTS

This work was supported by the Center for Functional Nanostructures (CFN) of the Deutsche Forschungsgemeinschaft (DFG) within project A2.

---

*Email Address: jurana.kvietkova@physik.uni-karlsruhe.de

[1] See, e.g., M. Klude and D. Hommel, Appl. Phys. Lett. **79**, 2523 (2001); H. Ishikura, T. Abe, N. Fukuda, H. Kasada, and K. Ando, *ibid.* **76**, 1069 (2000).

[2] H. Babucke, P. Thiele, T. Prasse, M. Rabe, and F. Henneberger, Semicond. Sci. Technol. **13**, 200 (1998).

[3] See, e.g., B. T. Jonker, Y. D. Park, B. R. Bennett, H. D. Cheong, G. Kioseoglou, and A. Petrou, Phys. Rev. B **62**, 8180 (2000).

[4] J. K. Furdyna, J. Appl. Phys. **76**, R29 (1988).

[5] O. Goede and W. Heimbrodt, Phys. Status Solidi B **146**, 11 (1988).

[6] A. Twardowski, T. Dietl, and M. Demianiuk, Solid State Commun. **48**, 845 (1983).

[7] K. J. Ma and W. Giriat, Solid State Commun. **60**, 927 (1986).

[8] J. Stankiewicz and J. R. Fermin, J. Appl. Phys. **63**, 3300 (1988).

[9] K. J. Ma and W. Giriat, Phys. Status Solidi A **95**, K135 (1986).

[10] R. B. Bylsma, W. M. Becker, J. Kossut, U. Debska, and D. Yoder-Short, Phys. Rev. B **33**, 8207 (1986).

[11] S. Adachi and T. Taguchi, Phys. Rev. B **43**, 9569 (1991).

[12] R. Dahmani, L. Salamanca-Riba, N. V. Nguyen, D. Chandler-Horowitz, and B. T. Jonker, J. Appl. Phys. **76**, 514 (1994).

[13] C. C. Kim and S. Sivananthan, Phys. Rev. B **53**, 1475 (1996).

[14] Y. D. Kim, S. L. Cooper, M. V. Klein, and B. T. Jonker, Phys. Rev. B **49**, 1732 (1994).

[15] W. K. Hung, M. Y. Chern, Y. F. Chen, W. C. Chou, C. S. Yang, C. C. Cheng, and J. L. Shen, Solid State Commun. **120**, 311 (2001).

[16] F. C. Peiris, S. Lee, U. Bindley, and J. K. Furdyna, J. Vac. Sci. Technol. B **18**, 1443 (2000).

[17] R. M. Azzam and N. M. Bashara, *Ellipsometry and Polarized Light* (North-Holland, Amsterdam, 1999).

[18] D. E. Aspnes, The Accurate Determination of Optical Properties by Ellipsometry, in E. D. Palik, *Handbook of Optical Constants of Solids* (Academic, New York, 1998) Vol. I, p. 89.

[19] G. E. Jellison, Thin Solid Films **313–314**, 33 (1998), and references therein. See also G. E. Jellison, "Ellipsometry data analysis", in *Handbook of Ellipsometry*, edited by G. E. Irene and H. W. Tompkins (Noyes Publictions, City, 2004).

[20] C. M. Herzinger, P. G. Snyder, B. Johs, and J. A. Woollam, J. Appl. Phys. **77**, 1715 (1995).

[21] S. Zollner, Appl. Phys. Lett. **63**, 2523 (1993).

[22] C. C. Kim, J. W. Garland, H. Abad, and P. M. Raccah, Phys. Rev. B **45**, 11749 (1992).

[23] C. C. Kim, J. W. Garland, and P. M. Raccah, Phys. Rev. B **47**, 1876 (1993).

[24] J. W. Garland, C. Kim, H. Abad, and P. M. Raccah, Phys. Rev. B **41**, 7602 (1990).

[25] S. Adachi, *Physical Properties of III-V Semiconductor Com-*

pounds (Wiley, New York, 1992); S. Adachi, T. Kimura, and N. Suzuki, J. Appl. Phys. **74**, 3435 (1993).

[26] M. S. Koo, T. J. Kim, M. S. Lee, M. S. Oh, Y. D. Kim, S. D. Yoo, D. E. Aspnes, and B. T. Jonker, Appl. Phys. Lett. **77**, 3364 (2000).

[27] R. Granger, J. T. Benhlal, O. Ndap, and R. Triboulet, Eur. J. Biochem. **13**, 429 (2000).

[28] K. Shahzad, D. J. Olego, and C. G. Van de Walle, Phys. Rev. B **38**, 1417 (1988).

[29] B. H. Lee, J. Appl. Phys. **41**, 2984 (1970).

[30] M. Hetterich, B. Daniel, C. Klingshirn, P. Pfundstein, D. Litvinov, D. Gerthsen, K. Eichhorn, and D. Speman, Prog. Solid State Chem. **1**, 649 (2004).

[31] H. Venghaus, Phys. Rev. B **19**, 3071 (1979).

[32] S. Lee, F. Michl, U. Rössler, M. Dobrowolska, and J. K. Furdyna, Phys. Rev. B **57**, 9695 (1998).